Computational evaluation of diarylbenzimidazole derivates as MEK inhibitors

Rašan, Lovro

UNIVERSITY OF RIJEKA

DEPARTMENT OF BIOTECHNOLOGY

Master's degree

''Medical chemistry''

Lovro Rašan

Computational evaluation of diarylbenzimidazole derivates as MEK inhibitors

Master's thesis

Rijeka, 2024.

UNIVERSITY OF RIJEKA

DEPARTMENT OF BIOTECHNOLOGY

Master's degree

''Medical chemistry''

Lovro Rašan

Computational evaluation of diarylbenzimidazole derivates as MEK inhibitors

Master's thesis

Supervisor: Dr.sc. Jurica Novak

Rijeka, 2024.

SVEUČILIŠTE U RIJECI

ODJEL ZA BIOTEHNOLOGIJU

Diplomski sveučilišni studij

''Medicinska kemija''

Lovro Rašan

Računalna evaluacija derivata benzimidazola kao inhibitora MEK

Diplomski rad

Mentor: Dr.sc. Jurica Novak

Rijeka, 2024.

The thesis was defended on February 22, 2024. year under the commission:

1. doc.dr.sc. Christian Reynolds
2. prof.dr.sc. Jasminka Giacometti
3. doc.dr.sc. Jurica Novak

The thesis containes 37 pages, 5 tables, 17 figures and 30 references.

Table of Content

List of Figures

List of Tables

Sažetak

Rak je stanje u kojem se određene tjelesne stanice nekontrolirano umnožavaju i napadaju druge dijelove tijela. Studija se bavi međumolekulskim interakcijama unutar signalizacijskog puta Raf/Ras/MEK/ERK, s MEK1 proteinom kao fokalnom točkom. Glavni cilj ove studije je istražiti 15 derivata diarilbenzimidazola kao potencijalne inhibitore MEK1 receptora, važne molekule u progresiji raka. Cilj je utvrditi njihovu učinkovitost i afinitete vezanja kroz različite analize, uključujući molekularno prijanjanje, simulacije molekularne dinamike te izračune slobodne energije vezanja. Strukturalna stabilnost kompleksa te interkacije kompleksa receptor-ligand potvrđena je praćenjem raznih parametara (RMSD, RMSF, RoG, SASA). Rezultati molekularnog prijanjanja indiciraju najjače veze između MEK1 i spojeva L05, L15 te referentnog Trametiniba. Na temelju rezultata molekularne dinamike i izračuna slobodne energije, L15 je potencijalni kandidat za lijek. Sljedeći korak je eksperimentalna validicija dobivenih rezultata računalne analize potencijalnih kandidata za lijek.

ključne riječi: MEK1, MAPK signalni put, diarilbenzimidazol derivati, Trametinib, molekularno prijanjanje, molekularna dinamika, slobodna energija vezanja

Abstract

Cancer is a condition where certain body cells uncontrollably multiply and invade other parts of the body. The study deals with molecular interactions within the Raf/Ras/MEK/ERK signalling pathway with the MEK1 as a focal point. The main goal of this study is to investigate diarylbenzimidazole derivatives as potential MEK1 inhibitors. The study evaluates 15 drug candidates designed to target the MEK1 receptor, an important biomolecule in cancer progression. The aim is to determine their effectiveness and binding affinities through various analyses, including docking, molecular dynamics simulations and free binding energy calculations. To provide insights into the structural stability and dynamic behavior of the drug-receptor complexes, several parameters were calculated (RMSD, RMSF, RoG, SASA). Compounds L05, L15 and referent Trametinib showed the best docking fit with the MEK 1 kinase. Based on the experimental values molecular dynamics and free binding energy, L15 is a potential drug candidate. Next step is to experimentally validate the obtained computational results of potential drug candidates.

key words: MEK1, MAPK pathyway, diarilbenzimidazole derivates, Trametinib, molecular docking, molecular dynamics, free binding energy

Chapter 1

Introduction

1.1 Introduction to cancer research

Cancer is a condition where certain body cells uncontrollably multiply and invade other parts of the body [1]. It has the potential to originate in any of the many cells comprising the human body and with a global mortality rate above 10 million deaths in the preceding year, cancer stands as the foremost cause of fatality on a global scale [2]. Surgery, chemotherapy, and radiation are the conventional methods used in cancer treatment, with chemotherapy playing a crucial role [3]. However, the effectiveness of drugs for cancer is limited due to the inability to target tumor cells specifically, leading to systemic toxicity and the emergence of drug-resistant cancer cells [4].

Targeted therapy has gained prominence in recent years due to its sensitivity towards cancer cells while sparing toxicity to off-target cells. The therapy's effectiveness lies in delivering treatments precisely to the affected area, thus minimizing unintended side effects on healthy tissues. It is often used in conjunction with chemotherapy and other cancer treatments, with the aim of inhibiting cancer cell growth, regulating the cell cycle, and triggering processes such as apoptosis or autophagy.

One example of a successful targeted cancer drug is Imatinib (Gleevec), a tyrosine kinase inhibitor approved by the FDA in 2001 [5]. Since then, there has been a growing development of similar small molecule drugs.

1.2 Cellular signaling pathway

Cellular signalling pathways are processes that enhance communication within and between cells, enabling them to respond to a multitude of external stimuli [6]. These pathways are intricately orchestrated networks of molecules and proteins that transmit information from the cell surface to the nucleus, ultimately influencing cellular behaviour and function [7]. This complex system is vital for regulating essential cellular processes such as growth, differentiation, proliferation, apoptosis, and response to environmental change [8]. Among these pathways, the Ras/Raf/ERK pathway, also known as the Mitogen-Activated Protein Kinase/Extracellular Signal-Regulated Kinase (MAPK/ERK) pathway, holds a prominent position due to its pivotal role in diverse physiological processes [9].

1.3 Mitogen-Activated Protein Kinase (MAPK) pathway

At its core, the Ras/Raf/MEK/ERK pathway is initiated by activating receptor tyrosine kinases (RTKs) or G protein-coupled receptors (GPCRs) in response to extracellular ligands, such as growth factors or cytokines. These receptors, upon ligand binding, activate the small GTPase protein Ras, which then sets in motion a downstream cascade of protein phosphorylation events [10]. Ras, in its Guanosine triphosphate (GTP)-bound active state, catalyzes the hydrolysis of GTP to guanosine diphosphate (GDP) and inorganic phosphate (Pi). Onwards Ras recruits and activates Raf kinases, including A-Raf, B-Raf, and C-Raf (Raf-1), leading to the phosphorylation and activation of Mitogen-Activated Protein Kinase Kinase (MEK or MAPKK). MEK, in turn, phosphorylates and activates the Extracellular Signal-Regulated Kinase (ERK) family of protein kinases, which include ERK1 and ERK2. Once activated, ERKs translocate to the nucleus, where they phosphorylate various transcription factors and modulate gene expression to elicit specific cellular responses [11]. Figure 1.1 illustrates this pathway.

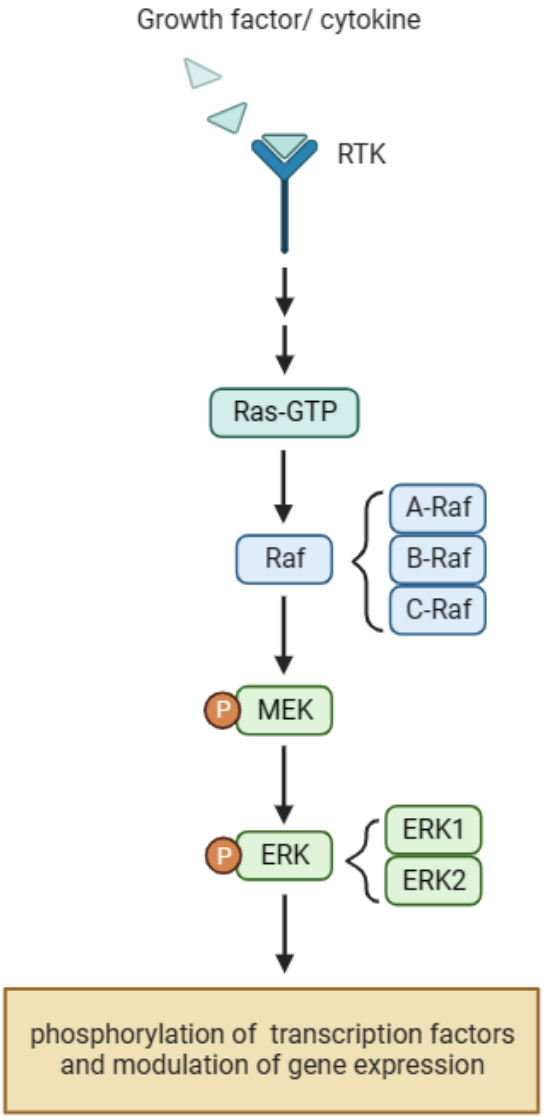

Figure 1.1: Activation cascade of Ras, Raf, MEK, and ERK proteins in response to extracellular ligands. The pathway starts with activating receptors, triggering a series of phosphorylation events, leading to modulation of gene expression and specific cellular responses. The figure was adopted from [12].

1.4 MEK1

MEK1, with its complex structure and tight regulation through phosphorylation and inhibition processes, is very important part of the MAPK/ERK signaling pathway. MEK1 acts as an intermediary kinase that phosphorylates and activates extracellular signal-regulated kinases 1 and 2 (ERK1/2), thus facilitating signal transduction from

cell surface receptors to the nucleus [7]. MEK1 is a dual-specificity kinase. Composed of several distinct domains it can phosphorylate both serine/threonine and tyrosine residues. *N*-terminal domain contains a regulatory region responsible for autoinhibition. In its inactive state, MEK 1 adopts a closed conformation due to the interaction of the *N*-terminal domain with the catalytic domain [12]. This autoinhibition prevents uncontrolled activation of downstream signaling. The catalytic domain contains the active site where MEK1 phosphorylates its substrates. It recognizes and phosphorylates the serine and threonine residues on ERK1/2, promoting their activation [12]. Although they have the same role and almost the same structure, MEK1 and MEK2 are not identical. MEK1 has a shorter activation loop (Figure 1.3, making it more flexible, while MEK2's longer activation loop offers greater stability. These distinctions influence their specific roles in cell signaling and phosphorylation cascades [10].

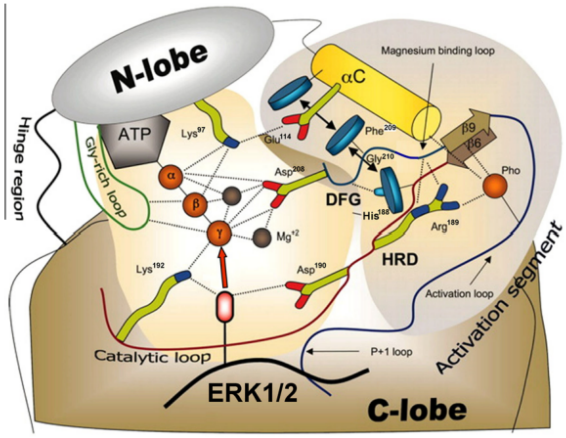

Figure 1.2: Display of the interactions between human MEK1 kinase catalytic core residues, ATP and ERK1/2. Catalytically important residues that are in contact with ATP and ERK occur within the light khaki background. Secondary structures and residues that are involved in the regulation of catalytic activity occur within the grey background. Figure was adopted from [12].

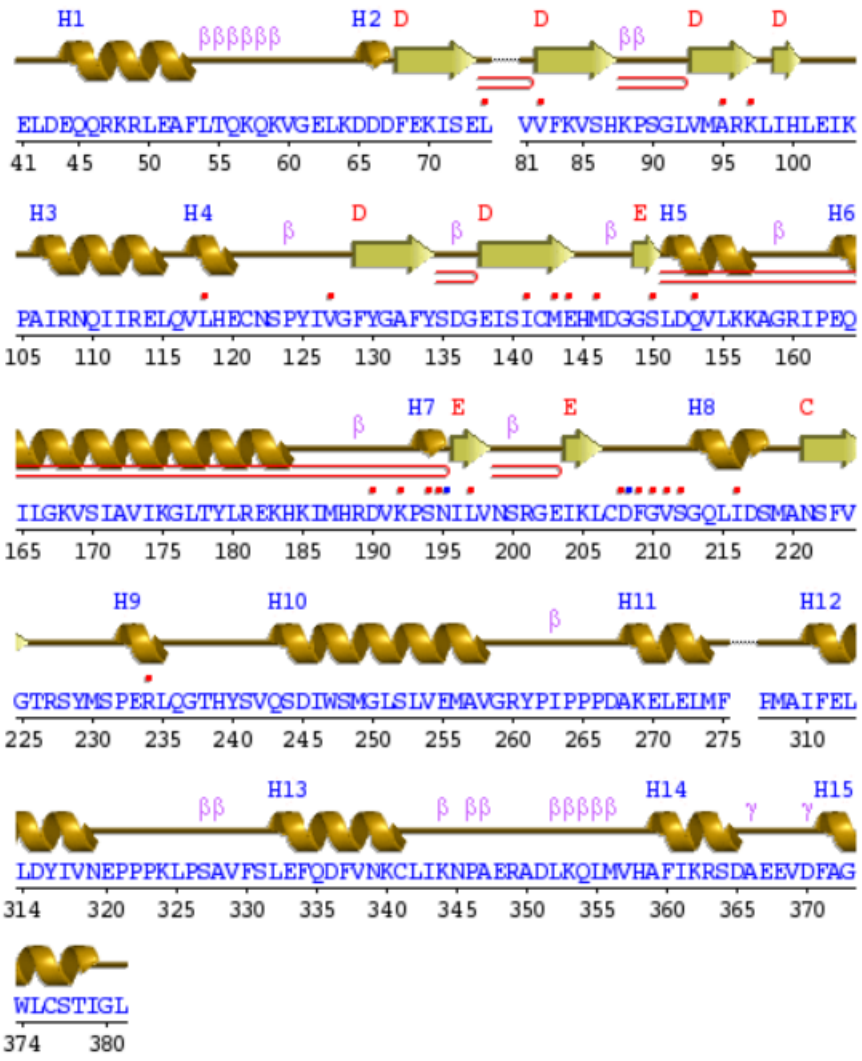

Figure 1.3: MEK1 chain C secondary structure. Figure was generated from pdbsum (`https://www.ebi.ac.uk/thornton-srv/databases/pdbsum/`). Helices labelled H1, H2, etc and strands by their sheets A, B, etc. β represent beta turns and γ gamma turns.

1.5 Diarylbenzimidazole derivates

The structural framework of diarylbenzimidazole derivatives is characterized by a benzimidazole core, a bicyclic aromatic system composed of a fused benzene ring and an imidazole ring (Figure 1.4). Attached to this core structure are two aryl groups, often bearing substituents that can be strategically modified to optimize binding affinity and selectivity [13]. This unique architecture imparts diarylbenzimidazole derivatives with the capability to interact with specific protein targets, making

them attractive candidates for drug discovery endeavors [14].

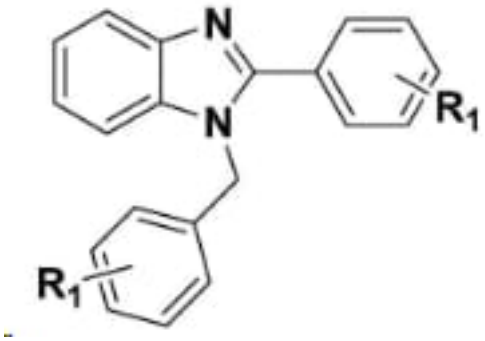

Figure 1.4: 2D structure of diarylbenzimidazole derivates

1.5.1 Tramatenib

Trametinib is classified as a second-generation small molecule that functions as an inhibitor of MEK kinase [15]. The compound exhibits allosteric properties and acts as an adenosine triphosphate (ATP) non-competitive inhibitor, with nanomolar potency against both MEK 1 and MEK 2 kinases. Its chemical structure features a pyridopyrimidine core fused with various functional groups (Figure 1.5A). The pyridopyrimidine moiety forms crucial hydrogen bonds within the MEK binding pocket, blocking downstream signalling, which is vital for cancer cell proliferation [16] (figure 1.5). Trametinib, a specific MEK inhibitor, has emerged as a beacon of hope in the battle against malignancies, demonstrating remarkable clinical efficacy in patients with specific mutations in the MAPK pathway, such as those found in melanoma [17]. By precisely blocking MEK1's catalytic activity, Trametinib curtails the unchecked cell growth that characterizes cancer, offering patients a chance for improved outcomes [18].

However, as with any targeted therapy, the story is not always straightforward. Genetic mutations within the target protein, in this case, MEK1, can significantly impact the drug's effectiveness, potentially leading to resistance or alternative responses [19]. Understanding how these activating and inactivating mutations influence Trametinib's binding to MEK1 at the molecular level is a critical step in optimizing treatment strategies and developing next-generation therapies.

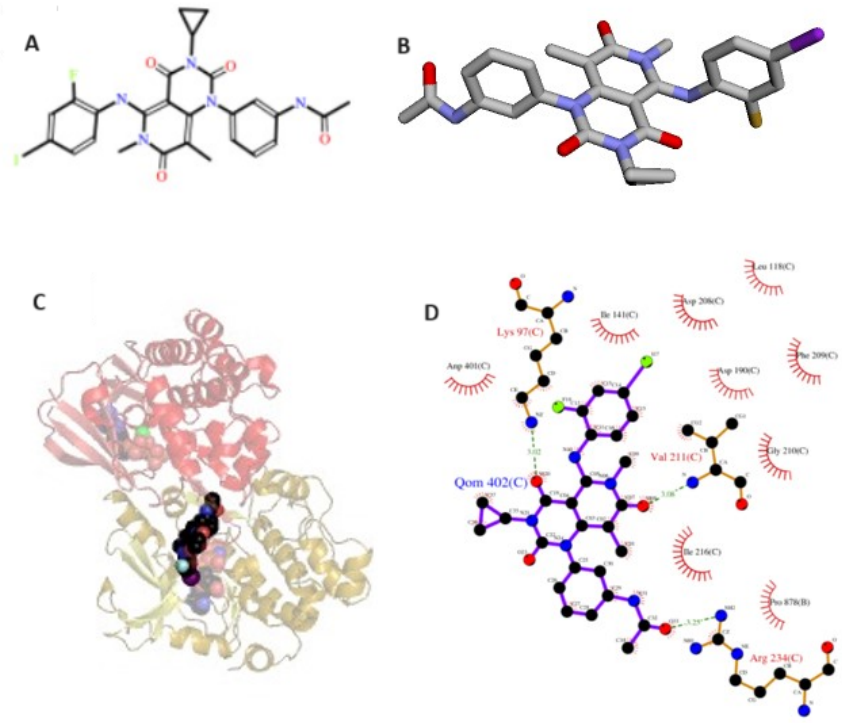

Figure 1.5: A) 2D structure of Trametinib, B) 3D structure of Trametinib, C) Trametinib in the catalytic site of the MEK1 protein (PDB ID:7jur), D) Trametinib in the catalytic site with bond-forming interactions with receptor residues. Figure was generated using PDBsum web server (`https://www.ebi.ac.uk/thornton-srv/databases/pdbsum/`)

1.6 Computational approach

Computational approaches have revolutionized drug research by significantly expediting the drug discovery process. Leveraging powerful algorithms and simulations, these methods allow researchers to analyze vast chemical databases, predict potential drug candidates, and understand molecular interactions. *In silico* techniques, such as molecular docking and virtual screening, expedite lead compound identification. Molecular dynamics simulations unveil dynamic behaviors of drug-target complexes. This data-driven approach optimizes drug design and reduces experimental costs and time [20].

Molecular docking

Molecular docking, involves the prediction of how small molecules, often drug candidates, bind to a target protein or receptor. Employing algorithms and scoring functions, molecular docking simulations explore various binding conformations, iden-

tifying the most energetically favorable binding modes[21]. A scoring function is a mathematical model or algorithm that quantifies the fitness of a given binding conformation by evaluating the interaction between the ligand and the receptor. These scoring functions are designed to calculate the binding affinity for a specific ligand-receptor complex. AutoDock Vina is widely used molecular docking software program. It incorporates a scoring function that takes into account various energy components, such as van der Waals interactions, electrostatic interactions, hydrogen bonding, and solvation effects. AutoDock Vina's scoring function aims to predict the binding free energy of a ligand-receptor complex, which is a crucial determinant of the likelihood of successful binding. The outcome of these studies not only elucidates the binding geometry but also provides critical insights into the strength and specificity of drug-target interactions [22].

Molecular dynamics

Following the docking phase, molecular dynamics simulations come into play, offering a dynamic perspective of the drug-receptor complex. Molecular dynamics allows exploration of the systems behavior over time, capturing the intricate motions and fluctuations of atoms and molecules [23]. This dynamic information is crucial for understanding the stability, flexibility, and conformational changes that may influence drug binding. A critical aspect of MD simulations is the ability to mimic the behavior of particles within a finite simulation cell while emulating the characteristics of an infinite and bulk-like environment. This transformational capability is achieved through the implementation of Periodic Boundary Conditions (PBC). PBC is crucial for avoiding boundary effects and accurately representing the collective behavior of particles in the system [24]. MD simulations provide a detailed insight into the system's temporal evolution by numerically solving Newton's equations of motion. These equations describe how particles in a system evolve over time by considering the forces acting upon them. In their simplest form, these equations can be expressed as:

$$F = ma \tag{1.1}$$

where *F* symbolizes the total force experienced by a particle, *m* signifies its mass, and *a* captures the acceleration it undergoes.

To mimic the behavior of particles in a realistic environment involves simulating systems in the temperature range. To simulate the effects of temperature and thermal fluctuations in MD, a Langevin dynamics (thermostat) is often used. It introduces a stochastic force, which mimics random collisions with the surrounding environment. The Langevin equation modifies Newton's equations by adding a damping term and

a random force to account for the system's interaction with a heat bath [25].

$$m\frac{d^2x(t)}{dt^2} = -\nabla U(x) - \gamma\frac{dx(t)}{dt} + \sqrt{2\gamma k_B T}R(t) \tag{1.2}$$

m represents the mass of the particle,
$x(t)$ is the position of the particle as a function of time,
$\nabla U(x)$ is the gradient of the potential energy function $U(x)$,
γ is the friction coefficient,
k_B is the Boltzmann constant,
T is the temperature,
$R(t)$ is a Gaussian-distributed random force term.

In systems with PBC, particles not only engage in interactions with their immediate neighbors but also interact with particles residing in neighboring periodic cells. These long-range interactions, particularly pronounced for charged particles under the influence of Coulomb's law, wield substantial influence over the system's overall behavior [24]. To compute long-range electrostatic interactions in MD simulations efficiently, the Ewald summation method dissects the electrostatic potential energy into two distinct components: a short-range term and a long-range term. The short-range component lends itself to straightforward computation by employing conventional pairwise interactions while adhering to a specified cutoff radius. In contrast, the long-range component presents a formidable computational task, necessitating a sophisticated representation in Fourier space [26]. To investigate the dynamic behavior of atoms and molecules over time such as complex interactions and movements of particles in various systems, analysis techniques like Root Mean Square Deviation (RMSD), Root Mean Square Fluctuation (RMSF), and Radius of Gyration are employed. RMSD measures the structural similarity between different configurations of a system by quantifying the average displacement of atoms from a reference structure. It is particularly useful in comparing the conformational changes in biomolecules over time [27].

$$\text{RMSD} = \sqrt{\frac{1}{M}\sum_{i=1}^{N} m_i \|\mathbf{X}_i - \mathbf{Y}_i\|^2} \tag{1.3}$$

Where:

RMSD is the Root Mean Square Deviation,
N is the number of atoms,
m_i is the mass of atom i,
M is the total mass,
$\mathbf{X}_i$ is the coordinate vector for target atom i,
$\mathbf{Y}_i$ is the coordinate vector for reference atom i,
$\|\cdot\|^2$ represents the squared Euclidean norm.

RMSF assesses the flexibility of individual atoms within a molecule during the simulation. It quantifies the deviation of atom positions from their average positions. This can be valuable in identifying regions of high mobility or rigidity [27].

$$\text{RMSF} = \sqrt{(\langle x_i^2 \rangle - \langle x_i \rangle^2)} \tag{1.4}$$

Where:

RMSF is the root mean square fluctuation
x_i denotes atomic positions and the averages are over all input frames i
$\langle \cdot \rangle$ denote an average over the ensemble of data points

The radius of gyration measures the compactness or spread of a molecule's structure. It calculates the root mean square distance of particles from the center of mass. A smaller radius of gyration indicates a more compact structure [27].

$$RoG = \sqrt{\frac{1}{N} \sum_{i=1}^{N} r_i^2} \tag{1.5}$$

Where: RoG = radius of gyration, N = total number of atoms, r_i = the distance of the i-th particle from the center of mass.

Molecular dynamics simulations bridge the gap between static docking poses and the dynamic reality of drug-target interactions [22].

Free energy calculations

Lastly, free energy calculations contribute a quantitative dimension to the triad, enabling the estimation of binding affinities and thermodynamic properties of the

protein-ligand system [28]. To calculate free energy, MD simulation uses techniques such as molecular mechanics/Poisson-Boltzmann surface area (MM/PBSA) and thermodynamic integration to provide insights into the energetic contributions governing drug binding.

MM/PBSA is a powerful computational technique used to estimate the binding free energy of a complex. It combines molecular mechanics, which describes the classical potential energy of a system, with Poisson-Boltzmann electrostatics and solvent-accessible surface area calculations to obtain a reasonably accurate estimate of the free binding energy [29].

The free binding energy (ΔG_{bind}) can be represented as:

$$\Delta G_{\text{bind}} = \Delta H - T\Delta S \approx \Delta E_{\text{MM}} + \Delta G_{\text{sol}} - T\Delta S \tag{1.6}$$

$$\Delta E_{\text{MM}} = \Delta E_{\text{internal}} + \Delta E_{\text{electrostatic}} + \Delta E_{\text{vdW}} \tag{1.7}$$

$$\Delta G_{\text{sol}} = \Delta G_{\text{GB}} + \Delta G_{\text{SA}} \tag{1.8}$$

Where:

ΔG_{bind} is the free binding energy

ΔH is the enthalpy change

T is the temperature in Kelvin

ΔS is the entropy change

ΔE_{MM} is the molecular mechanics energy change

ΔG_{sol} is the solvation free energy

$\Delta E_{\text{internal}}$ represents the change in internal energy

$\Delta E_{\text{electrostatic}}$ represents the change in electrostatic energy

ΔE_{vdW} represents the change in van der Waals energy

ΔG_{GB} represents the change in free energy calculated using the Generalized Born (GB) model

ΔG_{SA} represents the change in free energy due to the solvent-accessible surface area (SA).

Chapter 2

Aims

The scientific aim of this thesis is to comprehensively investigate and computationally evaluate diarylbenzimidazole derivatives as potential MEK inhibitors, with a primary focus on their interactions within the Raf/Ras/MEK/ERK signaling pathway. Amongst 15 potential drug candidates designed to target the MEK1 receptor as a pivotal biomolecule in cancer progression—the study aims to discern their binding affinities and efficacy through rigorous docking analyses. An essential facet involves a comparative evaluation with Tramatinib, an FDA-approved cancer drug, providing a benchmark for the effectiveness of the new candidates.

Beyond mere affinity assessment, the research investigates the molecular forces governing these interactions, elucidating the intricacies of binding mechanisms.

The ultimate goal is to expand the repertoire of viable cancer treatments. By pinpointing molecules exhibiting binding profiles akin to Tramatinib, the study not only diversifies therapeutic options but also stimulates further research in oncological drug discovery.

Chapter 3

Materials and methods

During the whole experiment for structure visualization and MD simulations vizualization Chimera 1.16 program was used.

3.1 Molecule preparation

3.1.1 Ligand preparation

In this study, a diverse set of structurally different serine/threonine binding compounds were chosen. The 3D structure of the ligands was determined by converting SMILES (Table 3.1) to 3D geometry and then optimizing the geometry in the novoprolabs site (https://www.novoprolabs.com/tools/smiles2pdb) To ensure the reliability and accuracy of the generated 3D structures, each compound was subjected to a visualization. For molecular docking preparation, it was essential to add hydrogen atoms to each ligand for accurate representations in simulations. This process was carried out using the AddH function in Chimera 1.16 program. Successful molecular docking simulations require determination of partial atomic charges and atom types. To meet these requirements, ligands were prepared using the AutoDock Tools program. The resulting files were saved in PDBQT (Protein Data Bank with charges and atom types) format. PDBQT-formatted files contain information regarding atom types, which are vital for determining atom parameters such as van der Waals radius.

Table 3.1: Compounds utilized througout this work.

Compound ID	SMILES
L01	BrC1=CC(C2=NC3=CC=CC=C3N2CC4=CC=CC(Br)=C4)=CC=C1
L02	ClC1=CC=CC=C1C2=NC3=CC=CC=C3N2CC4=CC=CC=C4Cl
L03	ClC(C=C1)=CC=C1C2=NC3=CC=CC=C3N2CC4=CC=C(Cl)C=C4
L04	BrC(C=C1)=CC=C1C2=NC3=CC=CC=C3N2CC4=CC=C(Br)C=C4
L05	O=[N+](C(C=C1)=CC=C1C2=NC3=CC=CC=C3N2CC4=CC=C([N+]([O-])=O)C=C4)[O-]
L06	CN(C)C(C=C1)=CC=C1C2=NC3=CC=CC=C3N2CC4=CC=C(N(C)C)C=C4
L07	O=[N+](C1=CC=CC=C1C2=NC3=CC=CC=C3N2CC4=CC=CC=C4[N+]([O-])=O)[O-]
L08	COC1=CC=CC=C1C2=NC3=CC=CC=C3N2CC4=CC=CC=C4OC
L09	COC1=CC=C(OC)C=C1C2=NC3=CC=CC=C3N2CC4=CC(OC)=CC=C4OC
L10	COC1=CC(OC)=CC=C1C2=NC3=CC=CC=C3N2CC4=CC=C(OC)C=C4OC
L11	COC(C(OC)=C1)=CC=C1C2=NC3=CC=CC=C3N2CC4=CC=C(OC)C(OC)=C4
L12	ClC1=CC(C2=NC3=CC=CC=C3N2CC4=CC=CC(Cl)=C4)=CC=C1
L13	ClC1=CC(Cl)=CC=C1C2=NC3=CC=CC=C3N2CC4=CC=C(Cl)C=C4Cl
L14	ClC1=CC=CC(Cl)=C1C2=NC3=CC=CC=C3N2CC4=C(Cl)C=CC=C4Cl
L15	C12=CC=CC=C1N=C(C3=CC(C=CC=C4)=C4C=C3)N2CC5=CC=C(C=CC=C6)C6=C5

3.1.2 Receptor preparation

The MEK1 macromolecule under investigation is represented by the PDB ID 7jur. This macromolecule was retrieved from the Research Collaboratory for Structural Bioinformatics (RCSB) Protein Database (https://www.rcsb.org/), and it serves as the focal point of our structural analysis. To initiate our analysis, specific regions of interest as ATP binding site and catalytic site within the protein were identified by referencing the relevant literature [10]. To accelerate the analysis, the protein chain that contains the catalytic site (chain C) was retained for further study, while the other chain B was removed. In preparation for molecular docking, various residues within the macromolecule as water molecules, phosphate groups, magnesium ions and any ligands initially present were eliminated. Determination of the protonation state of side chains within the macromolecule's amino acid residues was performed using the web-based Poisson Boltzmann tool (sever.poissonboltzmann.org/pdb2pqr). Calculations were conducted under physiological pH conditions (pH 7.4). When the structure was generated, essential components such as magnesium ion and phosphoaminophosphonic acid-adenylate ester (ANP) were reintroduced into the macromolecule structure using a text editor. The final preparation of the macromolecule for subsequent molecular docking studies was carried out using AutoDock Tools. In this step, Gasteiger charges were added to ensure accurate representation. The resulting prepared macromolecule was then saved in the PDBQT file format.

3.2 Molecular docking

Following the preparation of both ligands and the receptor, molecular docking was conducted to quantify the binding affinity and potential interactions between ligands and the 7jur receptor. The active binding site was identified based on the literature information. The center of this active site was precisely located at the Cartesian coordinates -53.20, 74.80, 10.80, and its cubic dimensions were defined as 20Åx20Åx20Å. To perform molecular docking simulations, AutoDock Vina was employed. Key parameters were set in config file to ensure the accuracy of the simulations. Specifically, the exhaustiveness and the number of modes were both configured to 100. Exhaustiveness refers to the degree to which a docking algorithm explores various potential binding poses or conformations of a ligand within a binding site on a protein or receptor. From the obtained docking results, two ligands displaying the lowest binding affinities and a control ligand Tramatenib were selected for further molecular dynamics simulations.

3.3 Molecular dynamics simulations

3.3.1 Ligand-receptor complex preparation

In the preparation of molecular dynamics (MD) simulations, positions of the ligand in the receptor active space were obtained through a molecular docking experiment. Positions with the lowest binding affinity were selected and taken for further analysis.

3.3.2 Ligands parametrization

In this study, we employed the Antechamber module from the AmberTools suite, along with the Parmchk utility, to parameterize the selected ligands. Antechamber is a powerful tool that utilizes the AM1-BCC (Antechamber Molecular Mechanics) charge model to derive force field parameters for small organic molecules. This module helps to determine the charges, atom types, and other necessary parameters required for MD simulations contained in mol2 file. After parametrization, it was crucial to ensure that ligands in this study were compatible with the force field using parmchk. Parametrization was performed on ANP molecule and ligands (L05, L15 and TRA).

3.3.3 MEK1-ligand complex building in explicit solvent

To ascertain the protonation state of histidine in a physiological pH environment, the H++ webserver (http://newbiophysics.cs.vt.edu/H++/) was used. All non-standard residues (magnesium ion, ANP and ligand) were placed into the downloaded protein. The construction of the protein system in an explicit solvent environment was executed using the LEaP module, an integral component of the AMBER molecular modeling suite. LEaP was instrumental in performing critical tasks, encompassing explicit solvation, charge neutralization, and the introduction of an appropriate salt buffer, facilitating the generation of a functional protein system.The ff19SB force field, representing the most recently updated AMBER force field tailored for protein was employed. GAFF force field was used for ANP and ligand molecules, TIP3P force field for water molecules and ions234l tip3p force fields for the magnesium ion. The charge of the protein was determined to be -2 at physiological pH. To maintain overall charge neutrality within the system, two Na+ ions were added to the system. Explicit solvation of the system was carried out using the LEaP command "SolvateOct". Complex was immersed in a solvent environment composed of pre-equilibrated TIP3P water molecules within a truncated octahedral periodic box. The dimensions of the solvation box were meticulously specified to ensure that every part of the protein complex remained at a minimum distance of 12.0 Å from the edges of the box. To emulate physiological conditions akin to cellular environments, a 150 mM NaCl salt buffer was introduced into the system. The quantities of sodium and chloride ions added were calculated based on the volume of the octahedral box generated in a previous step. 42 sodium and chloride ions were incorporated. Final structure goemetry of the solvated and neutralized complex is written in inpcrd file. MD simulation necessary data or topology of the system is written in prmtop file.

$$\text{concentration of } Cl^- \text{ ions} = \text{starting concentration} \times \text{Avogadro number} \times \text{Volume} \tag{3.1}$$

where:

$$\text{Concentration (mM)} = 150 \text{ mM starting concentration}$$
$$\text{Avogadro's Number} = 6.022 \times 10^{23} \text{ molecules/mol}$$
$$\text{Volume (L)} = \text{Volume of the solvation box L}$$

$$\text{Number of } Cl^- \text{ ions} = \big(\text{Volume (L)} \times \text{Concentration of } Cl^- \text{ ions}\big) \tag{3.2}$$

3.3.4 Relaxation of explicit solvent systems

In this section, relaxation of explicit solvent systems is conducted, specifically focusing on explicit water models for molecular dynamics (MD) simulations. To prepare the system for MD simulations, an initial minimization step is conducted to optimize the protein-ligand complex while keeping the protein fixed with a force constant of 10.0 kcal/mol/Å^2. The first minimization step is carried out to optimize water molecules in the system. During this step, no positional restraints are applied. The second minimization step is full relaxation. The maximum number of performed minimization cycles for both minimizations is set to 10,000 cycles with 4000 cycles of steepest descent and 6000 cycles of conjugate gradient. During the energy calculations, nonbonded interactions beyond 11Å are ignored. The heating step aims to gradually raise the temperature of the system to the desired simulation temperature. This process is performed in five steps (60 K for each step), increasing the temperature from an initial value to the target temperature of 310 K. For the temperature regulations, the Langevin thermostat was used with the collision frequency of $1\,\text{ps}^{-1}$. MD simulation will run 50000000 steps and each step is 2 fs. Total simulation time is 100ns. SHAKE algorithm involving hydrogen bonds stability during the simulation. The cut-off distance for nonbonded interactions is 11Å. MD simulations were conducted with AMBER package and on Issabela cluster at the University of Zagreb, Croatia. Processing coordinate trajectories and data files was performed in Amber package cpptraj.

Free binding energy calculations

The free binding energies (ΔG_{bind}) for a set of ligands (L15 and L5) and MEK1 were computed using a molecular mechanics/generalized Born surface area (MM/GBSA) protocol (as described in the Introduction). ΔG_{bind} calculations were conducted for the 2000 frames trajectory file that was split into 4 trajectory files 500 frames each. The final ΔG_{bind} was expressed as the average value $\pm$ the standard deviation across all segments. Additionally, the calculated MM/GBSA binding energies were dissected into specific contributions from individual residues. This analysis allowed for the identification of the impact of each amino acid side chain on ΔG_{bind}, revealing the changes in energy associated with interactions, solvation, and entropic contributions.

Chapter 4

Results

4.1 Molecular docking

The purpose of the molecular docking experiment was to predict and assess the binding affinity and ligand poses of a group of diarylbenzimidazole derivatives with MEK1 kinase. The binding energies, offer insights into the potential strength of the interaction between the compounds and the protein target. Generally, a more negative docking score indicates a stronger binding interaction. The Table 1.2 presents the docking scores and 2D structure of the molecule. For further molecular dynamics simulations, molecules of L15, L05, and TRA are used.

Table 4.1: Molecular docking results for diarylbenzimidazole derivatives in MEK1 protein, conducted in AutoDock Vina. Results are expressed as a binding affinity with the corresponding 2D structure.

Compound ID	Binding affinity/(kcal/mol)	2D structure
TRA	-9.6	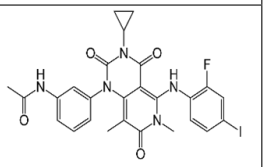
L15	-9.5	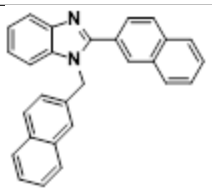
L05	-8.2	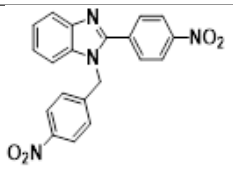
L12	-8.2	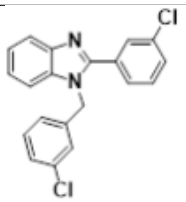
L13	-7.8	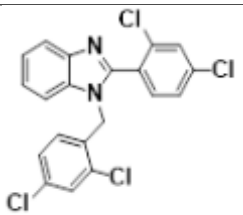
L07	-7.6	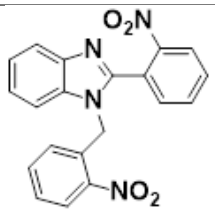

Compound ID	Binding affinity/(kcal/mol)	2D structure
L04	-7.5	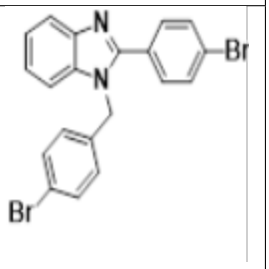
L11	-7.4	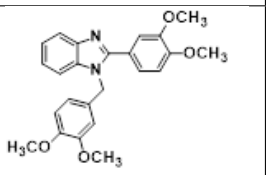
L10	-7.4	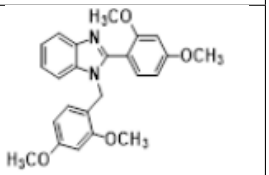
L06	-7.4	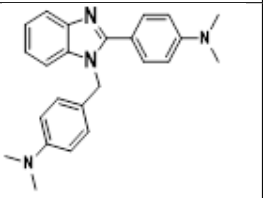
L03	-7.4	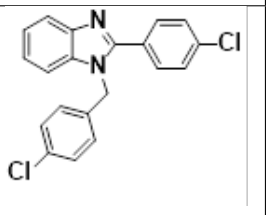

Compound ID	Binding affinity/(kcal/mol)	2D structure
L01	-7.4	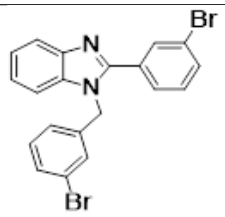
L08	-7.2	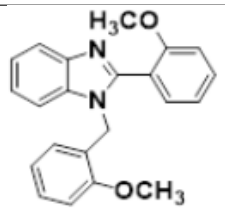
L09	-6.9	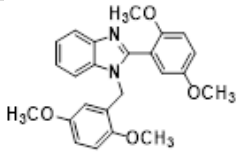
L02	-6.7	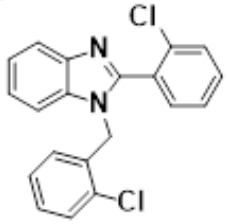
L14	-6.7	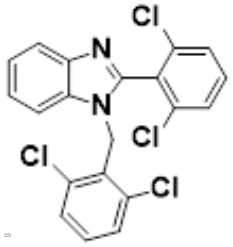

4.2 Molecular dynamics

To investigate conformational changes occurring during the simulation, RMSD values were calculated and compared with the initial structure. The results reveal minor structural rearrangements in the protein (Figure 4.1). The MEK-TRA complex had the smallest deviation range among the three complexes, with a maximum RMSD of 2.43 Å. The MEK-L15 complex had an average RMSD that was 0.02 Å higher than that of the MEK-TRA complex. The MEK-L05 complex had the greatest deviation range, ranging from 2.4 to 2.64 Å, with sharp peaks at 2.64 Å, 2.61 Å, and 2.60 Å.

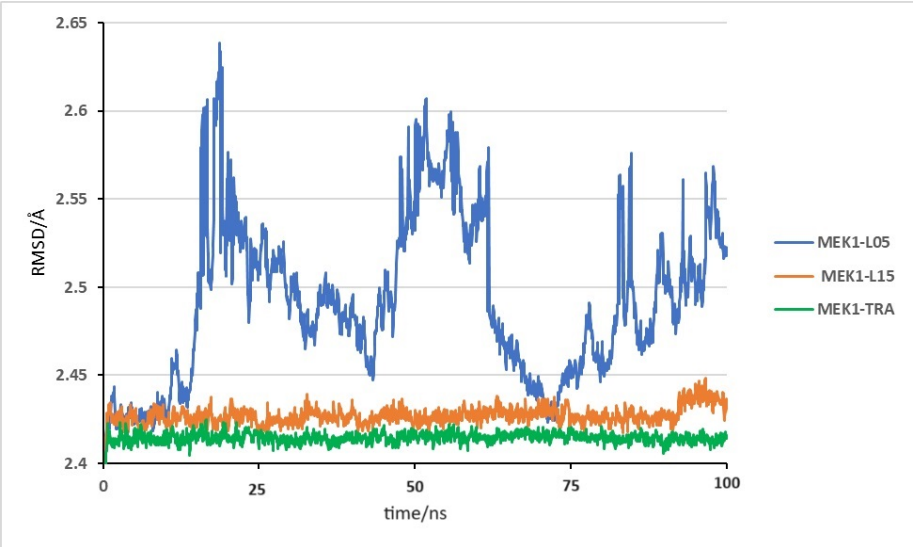

Figure 4.1: Variation of MEK1-ligand complex RMSD values throughout the molecular dynamics trajectory.

It has been observed that the RMSD values for the ligands are similar to those for the complex (Figure 4.2). Over the duration of the simulation, L15 and TRA have almost identical RMSD values. The TRA ligand shows a lower and more stable RMSD in time, with the maximum value being lower than 0.8 Å. However, L15 has a similar RMSD pattern to TRA but with a higher range of values (ranging from 0.2 to 0.9 Å) and more sharp peaks. On the other hand, L05 shows 0.5 Å higher average RMSD values than TRA and L15. Also, the range of RMSD for L05 is more than 1 Å.

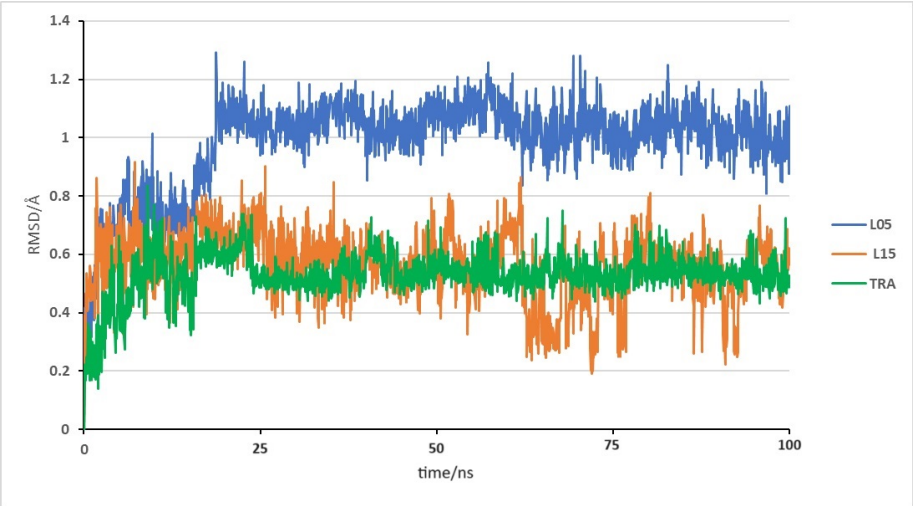

Figure 4.2: Variation of ligands (L15, L05 and TRA) RMSD values throughout the molecular dynamics trajectory.

The Root Mean Square Fluctuation (RMSF) values were calculated just for MEK1 protein with three different ligands (L05, L15, and TRA) excluded from the calculations. The results were then plotted to visualize the fluctuation profile of the protein (Figure 4.3). The MEK1 from the TRA complex exhibits relatively low RMSF values across all residues. In comparison, the MEK1 from the L15 complex shows slightly higher RMSF values, particularly in specific regions that correspond to more flexible regions of the protein structure. The MEK1 from the L05 complex displays substantially higher RMSF values than when paired with the other two ligands, with a higher fluctuation range.

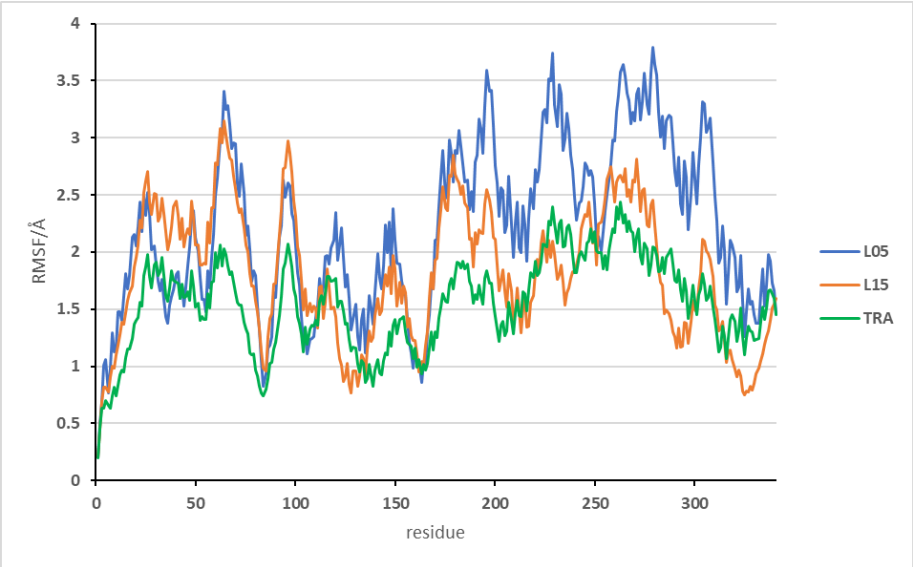

Figure 4.3: Atomic fluctuation profile of MEK1 protein (all ligands excluded).

Upon analysing MEK1-TRA and MEK1-L15, it was found that both components maintained relatively stable radius of gyration values throughout the simulation, with minor fluctuations. The radius of gyration values for MEK1-TRA ranged from approximately 19.80 to 20.50 Å, while MEK1-L15 exhibited a slightly wider range, spanning from about 19.80 to 20.80 Å. MEK1-L05 showed the most significant fluctuations within the broadest range over the course of the simulation. MEK1-L05 values ranged from about 19.80 to 20.80 Å (Figure 4.4).

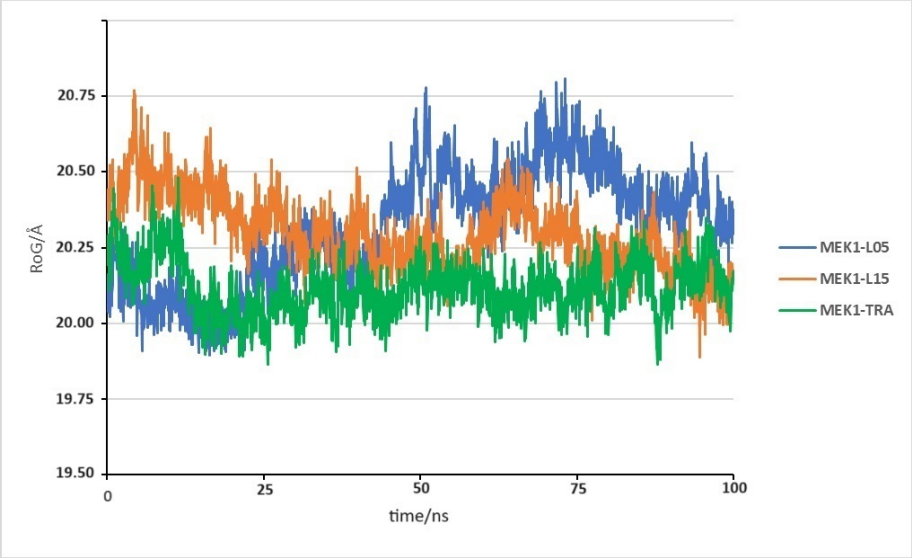

Figure 4.4: Variation of MEK1- ligand complex RoG values in the molecular dynamics simulation.

The solvent accessible surface area (SASA) values for the L05 receptor remain relatively stable across the simulation time, with occasional fluctuations but no discernible pattern of increase or decrease. On the other hand, L15 values display a noticeable pattern of variability across the simulation time. Moreover, the TRA receptor values show increasing variation, indicating a more dynamic surface exposure at this level. The fluctuations across frames are more pronounced in TRA receptors than in L05 and L15 receptors (Figure 4.5).

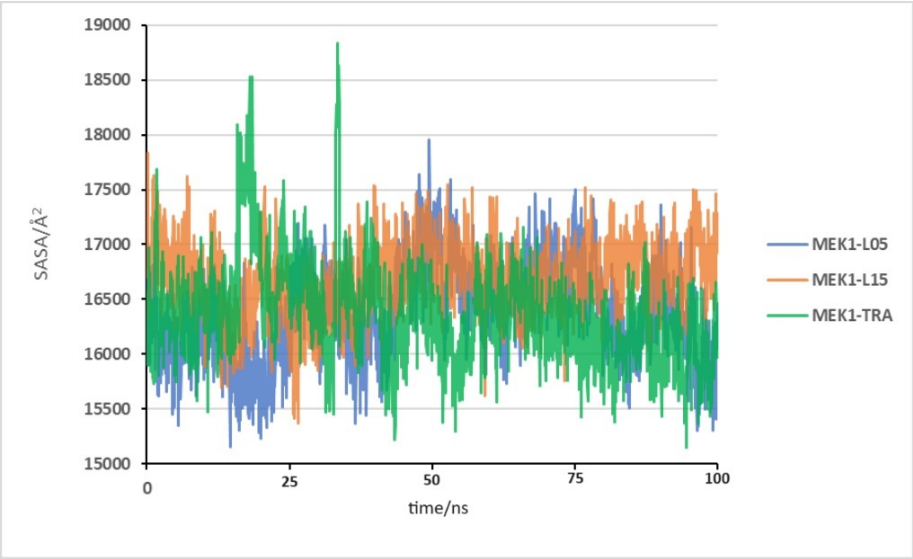

Figure 4.5: Variations of SASA values for MEK1-ligand complex throughout molecular dynamics trajectory.

There are no major deviations in statistical calculations from molecular dynamics for all analysed ligands. Minimal differences or some identical values exist between complexes. The standard deviation is also low, not greater than 0,53 for all calculations besides SASA (higher values) (Table 4.2).

Table 4.2: Statistical data for molecular dynamics calculations in Å

data	ligand	average	min	max	standard deviation
RMSD ligand	TRA	0.37	0.21	0.53	0.23
	L15	0.39	0.21	0.58	0.26
	L05	0.73	0.31	1.11	0.53
RMSD complex	TRA	2.42	2.41	2.43	0.03
	L15	2.44	2.42	2.44	0.07
	L05	2.52	2.42	2.64	0.16
RMSF	TRA	1.53	0.61	2.41	1.14
	L15	1.95	0.64	3.16	1.62
	L05	2.32	0.72	3.41	2.46
RoG	TRA	20.20	19.85	2.48	0.25
	L15	20.32	19.86	2.76	0.21
	L05	20.26	19.91	2.78	0.16
SASA/Å^2	TRA	16701.62	15152.72	18889.47	81.81
	L15	16488.44	15473.37	17836.61	62.65
	L05	16268.92	15140.37	17963.43	75,20

The fluctuation of hydrogen bonds over time can be seen in (Figure 4.6). The total number of donor and acceptor hydrogen bonds for the receptor and ligand in the analyzed complexes show only minor deviations. The range of hydrogen bonds varies

from 3 to 15 between each ligand-receptor complex. MEK1-TRA and MEK1-L15 display a more stable values of hydrogen bonds over time than MEK1-L05. MEK1-TRA has the highest in average hydrogen bond connections with 7.26 bonds. On average, MEK1-L15 creates 0.32 fewer hydrogen bonds than MEK1-TRA, while MEK1-L05 creates 0.58 fewer.

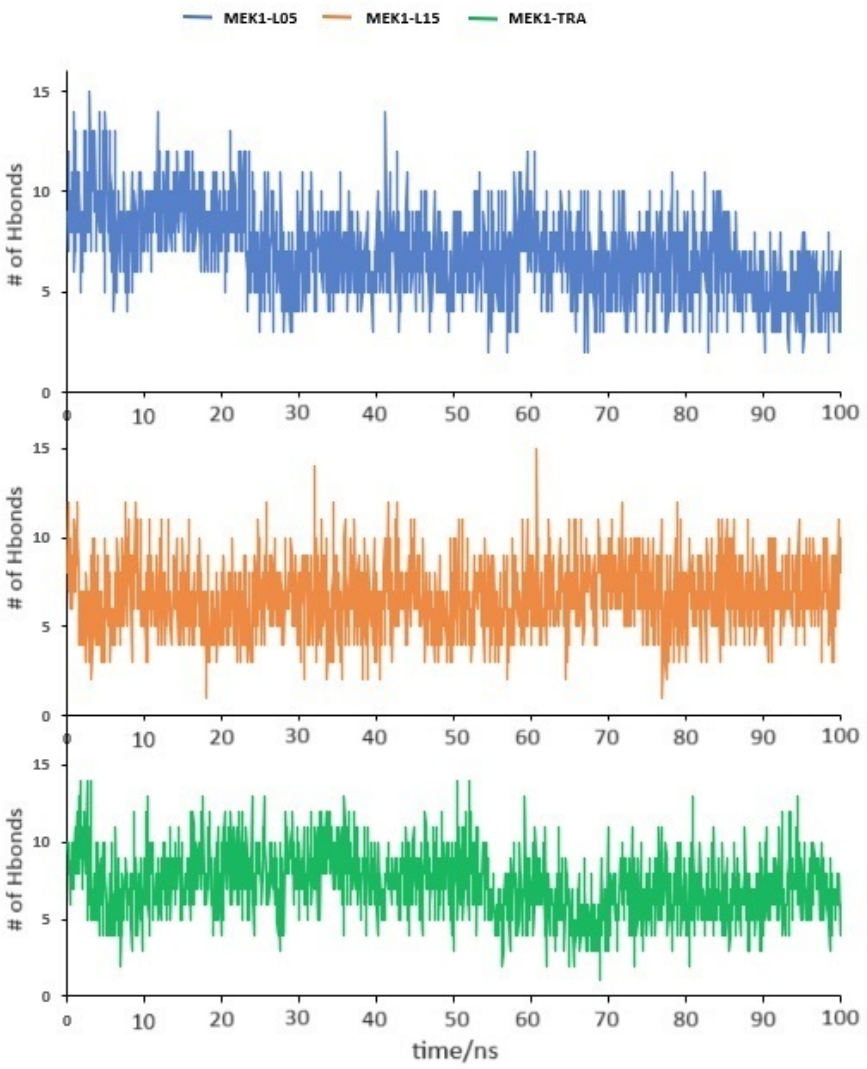

Figure 4.6: The sum of total hydrogen bonds during the molecular dynamics simulation for MEK1-L05, MEK1-L15, MEK1-TRA.

Calculating secondary structure allows analyzing the evolving three-dimensional structures of these molecules during simulations. Figure 4.7 shows the stability of secondary structure elements for MEK1 protein of MEK1-ligand complexes throughout simulation time. MEK1 in MEK1-TRA and MEK1-L15 complexes shows slight structural changes per frame. Most changes are between residues Gln243 - Val258. 3-10 helix (H10 on Figure 1.3 structures are turning into beta turns. From residue Glu163 - His184 H6 alpha helix secondary structures turn into beta turns and 3-10 helix structures. MEK1 in MEK1-L05 contain structural changes on the same spots but there is a low range of residues with secondary structure changes.

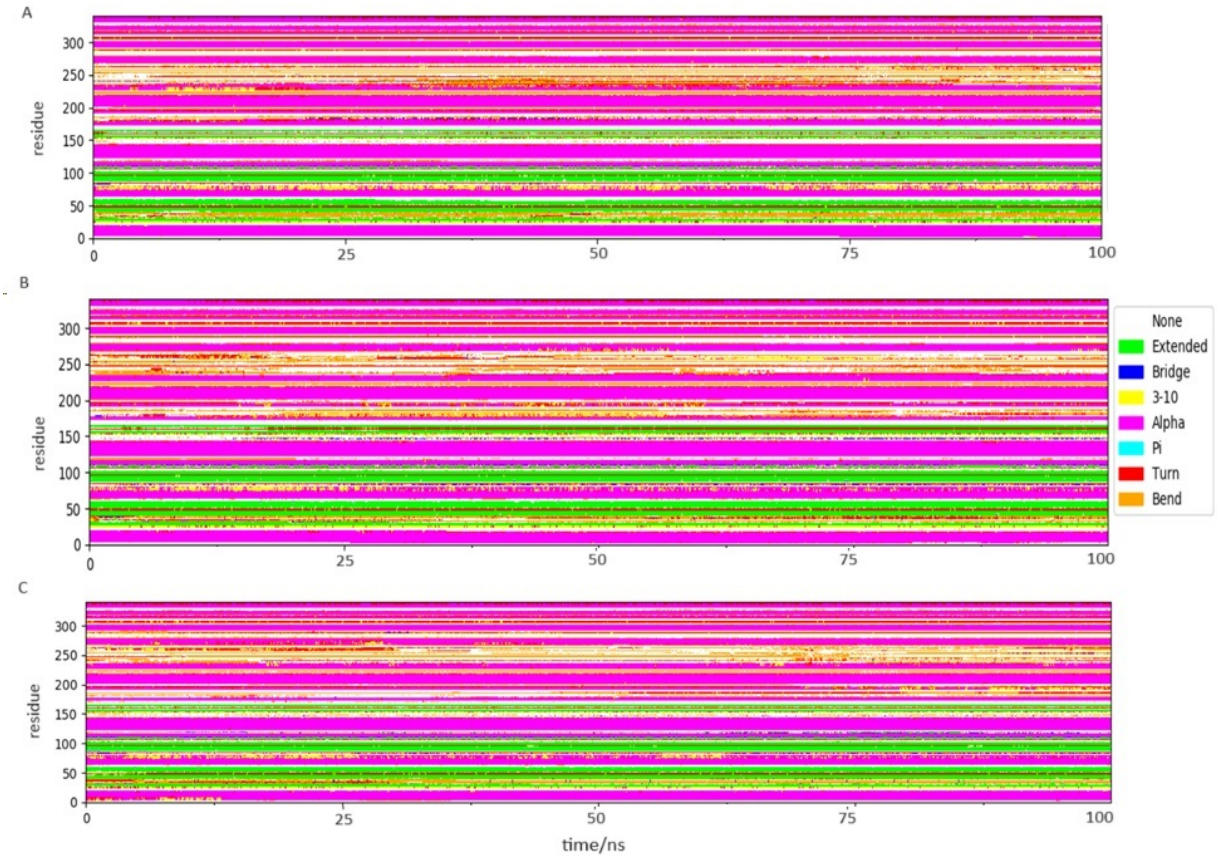

Figure 4.7: Secondary structure plot for MEK1 protein throughout the molecular dynamics simulation. A)MEK1-L15 protein, B) MEK1-TRA protein, C) MEK1-L05 protein.

To obtain insights into the free binding energy (ΔG_{bind}), we analyzed the energy components for L05 and L15 (Table 4.3). The data for TRA free binding energy were taken from the literature [30]. Based on the data, it can be inferred that TRA has the lowest values for both ΔG_{bind} and $T\Delta S$. L15 has slightly higher values for ΔG_{bind} compared to TRA, while L05 has values that are three times higher than TRA's. The entropic contribution ($T\Delta S$) of L15 and L05 are quite similar, whereas TRA has a significantly smaller value.

Table 4.3: Average calculated free energy calculations and standard deviation for MEK1-L05 and MEK1-L15 complexes in kcal/mol. MEK1-TRA* values were taken from reference [30]

energy component	MEK1-L05	MEK1-TRA*	MEK1-L15
$\Delta E_{(}(vdW)$	-45.1 ± 3.1	-54.6 ± 4.9	-61.1 ± 2.7
$\Delta E_{\text{electrostatic}}$	-8.3 ± 4.6	-85.0 ± 10.4	-7.7 ± 2.9
ΔG_{GB}	30.1 ± 4.5	90.1 ± 13.6	27.1 ± 2.1
ΔG_{SA}	-5.7 ± 0.3	-5.6 ± 2.0	-6.9 ± 0.2
ΔG_{gas}	-53.4 ± 5.7	No data	-68.8 ± 4.1
ΔG_{solv}	24.5 ± 4.4	No data	20.1 ± 2.1
$T\Delta S$ (T=310.0K)	-22.7 ±6.6	-60.2 ± 5.5	-24.2 ± 5.5
ΔG_{bind}	-28.9 ± 3.1	-55.0 ± 3.9	-48.7 ± 3.2

The MM/GBSA method for binding free energy decomposition was used to identify the important amino acid residues that play a crucial role in the binding of the ligand to the protein. To classify which residues have a dominant contribution, a threshold of -1.5 kcal/mol was set for the free energy of binding of a single residue. In the case of MEK1-L05 and MEK1-TRA, Ile59 and Ile101 respectively had the lowest free binding energies, less than -2.5 kcal/mol. For both MEK1-L05 and MEK1-L15 complexes, Ile176 and Met175/Leu179 had a notable contribution to free binding energy. The MEK1-L15 complex also had additional residues including Leu78, Cys167, and Phe169, which had higher ΔG_{bind} (Table 4.4).

Table 4.4: Contributions of the most important amino acid residues for the binding L05 and L15 to MEK1 protein.

MEK1-L05		MEK1-L15	
Residue	ΔG_{bind}/kcal/mol	Residue	ΔG_{bind}/kcal/mol
Ile59	-2.7	Ile101	-2.7
Leu175	-2.5	Leu175	-2.1
Met179	-2.4	Leu78	-1.9
Ile176	-1.9	Ile59	-1.8
Leu175	-1.7	Leu78	-1.7
Ile101	-1.5	Cys167	-1.5
		Phe169	-1.6

Chapter 5

Discussion

5.1 Molecular docking

The results of docking analysis showed varying binding affinities among the diarylbenzimidazole derivatives. Trametinib, a known MEK inhibitor, was used as a reference ligand and showed the highest binding affinity with a score of -9.6 kcal/mol. L15 also exhibited a strong binding interaction with MEK1 kinase with a score of -9.5 kcal/mol, which makes it an excellent candidate for further investigation. L05 and L12 showed moderate binding affinities with docking scores of -8.2 kcal/mol, indicating potential inhibitory activity against MEK1 kinase. In contrast, L13, L07, and L04 exhibited slightly weaker interactions with binding energies of -7.8, -7.6, and -7.5 kcal/mol, respectively. The ligands with docking scores of -7.4 kcal/mol (L11, L10, L06, L03 and L01) and -7.2 kcal/mol L08, indicate similar but relatively moderate binding affinities.

L09, L02, and L14 displayed weaker binding affinities with docking scores of -6.9, -6.7, and -6.7 kcal/mol, respectively. It is essential to consider both the strength of binding interactions and the molecular dynamics data of these interactions for the development of effective MEK inhibitors. While L15, L05 and TRA exhibit strong binding affinities, their molecualr dynamics need to be evaluated to determine their effectiveness as MEK inhibitors.

5.2 Molecular dynamics

The investigation into conformational changes during the simulation, as assessed through RMSD values of their comparison with the initial structure, has provided valuable insights into the dynamic behavior of the protein. The results indicate that the protein undergoes minor structural rearrangements, as illustrated in Figure 4.1. Stable RMSD values towards the end of the simulation prove that are system is in equilibrium and data is valid. Notably, the MEK-TRA complex exhibits the smallest deviation range among the three complexes, with a maximum RMSD of 2.43 Å. In contrast, the MEK-L15 complex demonstrates a slightly higher average RMSD, differing by 0.02 Å compared to the MEK-TRA complex. The MEK-L05 complex displays the most extensive deviation range indicating larger conformational changes in loop structures during the simulation which is visible on Figure 4.1. Most diverse structural changes are on the outside of the protein and do not have a major impact on the active site which is crucial for ligand binding (Figure 5.1).

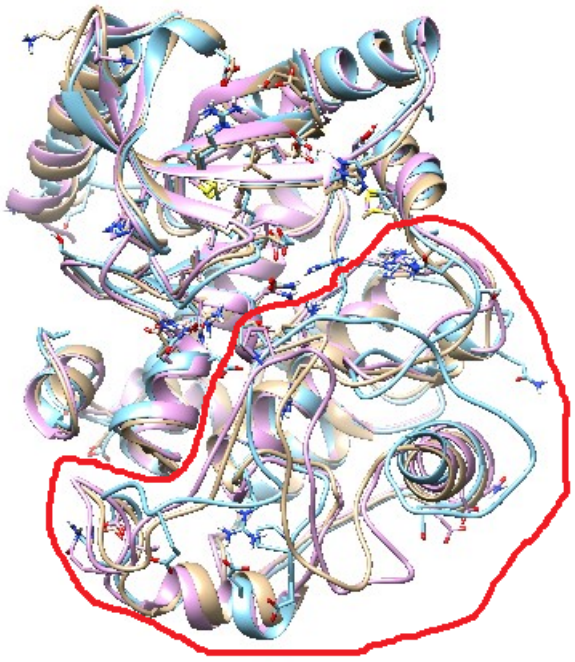

Figure 5.1: Deviation of loop regions of MEK1 secondary structure made using Chimera 1.16 clustering after MD simulation.

The RMSD analysis of the ligands and the complex demonstrates that the ligands stability is overall similar to that of the complex. However, each ligand exhibits unique patterns of structural deviations. TRA stands out as the most stable ligand,

with the lowest and most consistent RMSD values, while L15 exhibits similar stability but with more pronounced fluctuations. L05, on the other hand, demonstrates lower stability, with higher average deviation values and a broader range of structural changes. Most severe change is rotation of a C atom that connects nitrobenzene group (Figure 5.2). Each ligand RMSD values are lower then protein-ligand values which indicates none of the ligands has difused away from its initial binding site.

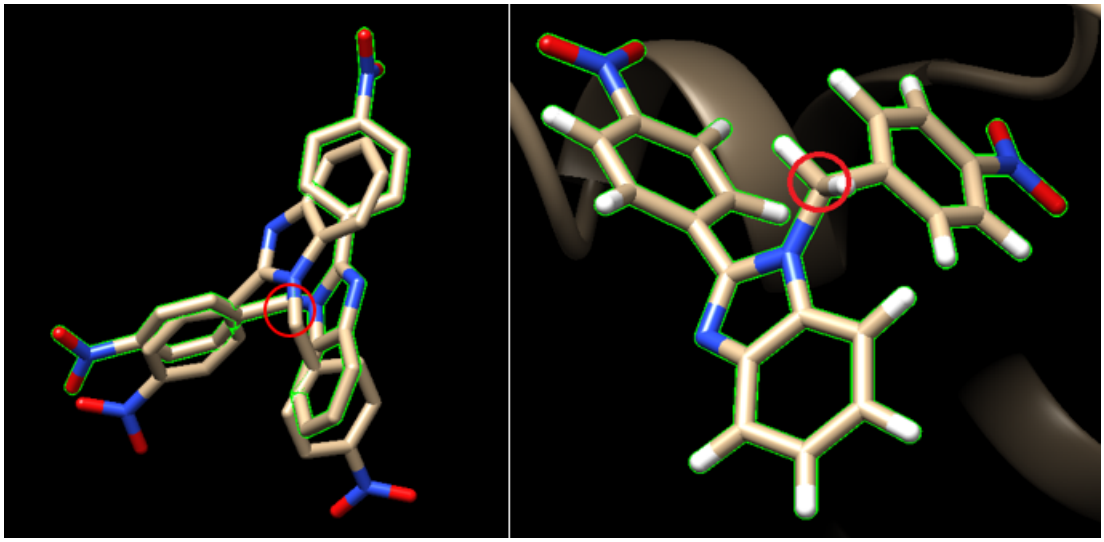

Figure 5.2: A) The difference in two L05 structures deviations B) C atom rotation (red circle) holding nitrobenze group of L05 in MEK1 active spot. Figure was generated in Chimera 1.16.

The MEK1 protein from the TRA complex exhibited relatively low RMSF values across all residues. The low RMSF values in the TRA complex imply that the protein maintains a more rigid and stable conformation when bound to this ligand. In contrast, the MEK1 protein in the L15 complex displayed slightly higher RMSF values compared to the TRA complex. In MEK1 protein of the MEK1-L05 complex, the RMSF values were substantially higher than when paired with the other two ligands. The higher RMSF values across all residues and a broader fluctuation range indicate that the L05 ligand significantly enhances the flexibility and dynamic behavior of the MEK1 protein. These elevated RMSF values were particularly prominent in specific regions as a loop regions, which correspond to inherently flexible regions of the protein structure. Alpha helix and beta sheets are more rigid part of the protein (Figure 5.1). The lowest RMSF values are displayed on residues Leu78, Ile101, Cys167, Phe169 and Leu175. All of the residues are ligand-binding residues (Figure 5.3).

MEK1 in complex with TRA and L15 exhibited relatively stable RoG values throughout the simulation, with minor fluctuations. A stable RoG over time suggests that the ligands maintain a specific overall shape indicating that the protein's structural compactness was well-maintained during the simulation. TRA causing the least change

in RoG might have a more specific interaction with the protein. In contrast, MEK1 in complex with L05 displayed the more significant fluctuations in RoG values, indicating structural changes throughout the simulation (Figure 5.1).

The SASA values presented in Figure 4.5 provide insights into low protein conformational changes, flexibility, and potential binding sites. There are no significant differences in any analyzed values which indicates that MEK1 protein surface is constant throughout molecular dynamic simulation. The SASA values are consistent with the RMSD complex and RoG values.

Hydrogen bond calculations help to understand structural stability, protein-ligand binding, and conformational changes in complex structures. Our analysis of hydrogen bonds show stable fluctuation over time within the MEK1-TRA, MEK1-L15, and MEK1-L05 complexes. MEK1-TRA's consistent and high average hydrogen bond count suggests a stable interaction. In the active spot only TRA produce hydrogen bonds with MEK1 residues Lys57, Asp168, Val171 and Ser172 Figure 5.3). L15 and L05 produces weak hydrophobic or aromatic bonds with the MEK1 (Figures 5.4 and 5.5).

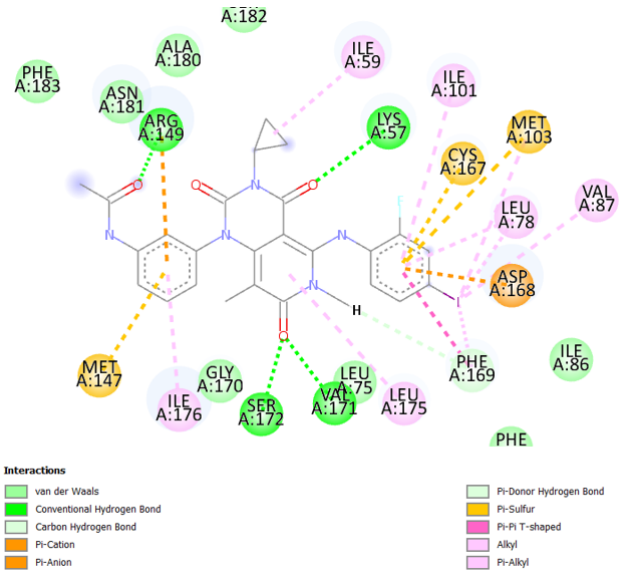

Figure 5.3: Display of 2D MEK1-TRA binding spot interactions. The figure was generated in DS Visualizer program.

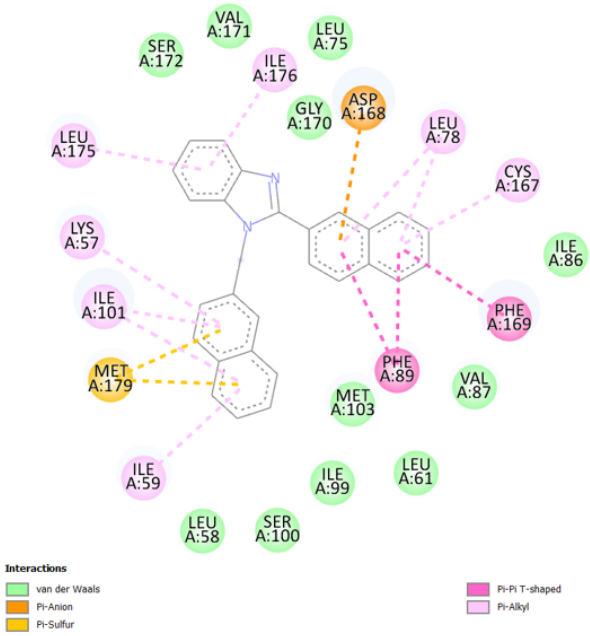

Figure 5.4: Display of 2D MEK1-L15 binding spot interactions. The figure was generated in DS Visualizer program.

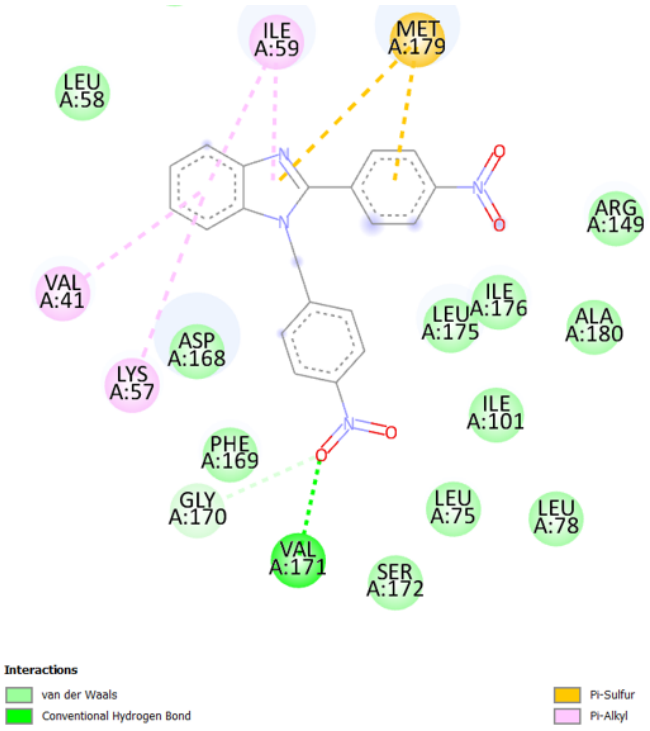

Figure 5.5: Display of 2D MEK1-L05 binding spot interactions. The figure was generated in DS Visualizer program.

The secondary structure analysis indicated that MEK1 in all complexes exhibited relatively minor structural changes during the simulation. These changes were primarily localized to specific regions between residues Gln243 - Val258 3-10 helix and Glu163 - His184 alpha helix. These observations suggest that the binding of TRA and L15 ligands did not significantly perturb the overall secondary structure of MEK1. On the other hand, MEK1 in the MEK1-L05 complex exhibited more pronounced structural changes over the simulation time. Notably, these changes occurred in the same regions as those observed in the MEK1-TRA and MEK1-L15 complexes, around residues Gln243 - Val258 3-10 helix and Ile99 - His100 strand, and Glu163 - His184 alpha helix (Figure 1.3). However, in the case of MEK1-L05, the changes were not limited to specific residues; instead, they affected a wider range of residues with alterations in secondary structure. These findings suggest that the choice of ligand has a distinct impact on the conformational dynamics of MEK1. All ligands induce only minor perturbations in the secondary structure. Based on the previously calculated RMSD there are no significant deviations and consequently mild structural changes. Ligand-induced structural changes in proteins can affect their biological functions, and such knowledge is essential for rational drug design and development.

5.3 Free binding energy calculations

The negative total ΔG total and favorable individual energy components ΔE_{vdW} and $\Delta E_{\text{electrostatic}}$ suggest that binding to L15 is energetically favorable. The positive ΔG_{GB} and negative ΔG_{SA} components indicate a balance between polar and nonpolar interactions in the solvation process. The contributions of ΔS and enthalpy provide insights into the thermodynamics of binding. The significant positive solvation contribution indicates that the binding process is largely driven by solvent interactions. The values of ΔG for the L15 complex are more favorable than those of L05, indicating that L15 has a stronger binding to the MEK1 receptor, as expected from previous calculations.

MM/GBSA decomposition is a useful tool for understanding the various forces and interactions that contribute to the binding of a ligand to a receptor. Residues with lower ΔG_{bind} values contribute to stronger ligand binding in the receptor's active site. Specifically, Ile59, Leu175, Ile176, and Ile101 create hydrophobic interactions with the aromatic functional groups in L05 and L15. Met179 in the L05 complex and Phe169 in the L15 complex can also create aromatic bonds between the receptor and the ligand (Figures 5.3, 5.4 and 5.5). These interactions also affect protein fluctuation which is visible in Figure 4.3.

Chapter 6

Conclusion

This study highlights the importance of not only the strength of binding when developing effective MEK inhibitors. A combination of molecular docking, molecular dynamics simulations and free binding energy calculations provided a comprehensive understanding of the diarylbenzimidazole derivatives' binding affinities, structural stability, and dynamic behaviour with MEK1 kinase. These findings are crucial for the rational design of MEK inhibitors. Based on the poor results of molecular docking and molecular dynamics, we can conclude that L05 is not a potential candidate for further research. On the other hand, L15 exhibits similar results to a control ligand TRA and stands out as a promising candidate for further investigation. Free binding energy calculations confirm the results. After completing *in silico* calculations, the next step is to synthesize L15 for further development as a potential drug.

Bibliography

[1] Tanja Šarenac and Momir Mikov. Cervical cancer, different treatments and importance of bile acids as therapeutic agents in this disease. *Frontiers in Pharmacology*, 10:484, 2019.

[2] Kalirajan Rajagopal, Anandarajagopal Kalusalingam, Anubhav Raj Bharathidasan, Aadarsh Sivaprakash, Krutheesh Shanmugam, Monall Sundaramoorthy, and Gowramma Byran. In silico drug design of anti-breast cancer agents. *Molecules*, 28(10):4175, 2023.

[3] Guang Xu and Howard L McLeod. Strategies for enzyme/prodrug cancer therapy. *Clinical Cancer Research*, 7(11):3314–3324, 2001.

[4] Viswanadha Vijaya Padma. An overview of targeted cancer therapy. *BioMedicine*, 5:1–6, 2015.

[5] U.S. Food and Drug Administration. Information on gleevec (imatinib mesylate).

[6] Jerry L Wilson. Biochemistry; (stryer, lubert), 1988.

[7] Robert Roskoski Jr. Erk1/2 map kinases: structure, function, and regulation. *Pharmacological research*, 66(2):105–143, 2012.

[8] Bruce Alberts. *Molecular biology of the cell*. Garland science, 2017.

[9] Ahmed A Samatar and Poulikos I Poulikakos. Targeting ras–erk signalling in cancer: promises and challenges. *Nature reviews Drug discovery*, 13(12):928–942, 2014.

[10] Robert Roskoski. Mek1/2 dual-specificity protein kinases: Structure and regulation. *Biochemical and Biophysical Research Communications*, 417(1):5–10, 2012.

[11] Patrick J Roberts and Channing J Der. Targeting the raf-mek-erk mitogen-activated protein kinase cascade for the treatment of cancer. *Oncogene*, 26(22):3291–3310, 2007.

[12] Robert Roskoski Jr. Mek1/2 dual-specificity protein kinases: structure and regulation. *Biochemical and biophysical research communications*, 417(1):5–10, 2012.

[13] Yunqi Li, Chunyan Tan, Chunmei Gao, Cunlong Zhang, Xudong Luan, Xiaowu Chen, Hongxia Liu, Yuzong Chen, and Yuyang Jiang. Discovery of benzimidazole derivatives as novel multi-target egfr, vegfr-2 and pdgfr kinase inhibitors. *Bioorganic & medicinal chemistry*, 19(15):4529–4535, 2011.

[14] Keith T Flaherty, Caroline Robert, Peter Hersey, Paul Nathan, Claus Garbe, Mohammed Milhem, Lev V Demidov, Jessica C Hassel, Piotr Rutkowski, Peter Mohr, et al. Improved survival with mek inhibition in braf-mutated melanoma. *New England Journal of Medicine*, 367(2):107–114, 2012.

[15] Zaigham M Khan, Alexander M Real, William M Marsiglia, Arthur Chow, Mary E Duffy, Jayasudhan R Yerabolu, Alex P Scopton, and Arvin C Dar. Structural basis for the action of the drug trametinib at ksr-bound mek. *Nature*, 588(7838):509–514, 2020.

[16] Robert Zeiser, Hana Andrlová, and Frank Meiss. Trametinib (gsk1120212). *Small Molecules in Oncology*, pages 91–100, 2018.

[17] John R Fabian, Ira O Darr, and Deborah K Morrison. Critical tyrosine residues regulate the enzymatic and biological activity of raf-1 kinase. *Molecular and cellular biology*, 13(11):7170–7179, 1993.

[18] Robert Zeiser. Trametinib. *Small Molecules in Oncology*, pages 241–248, 2014.

[19] Caroline M Emery, Krishna G Vijayendran, Marie C Zipser, Allison M Sawyer, Lili Niu, Jessica J Kim, Charles Hatton, Rajiv Chopra, Patrick A Oberholzer, Maria B Karpova, et al. Mek1 mutations confer resistance to mek and b-raf inhibition. *Proceedings of the National Academy of Sciences*, 106(48):20411–20416, 2009.

[20] Douglas B Kitchen, Hélène Decornez, John R Furr, and Jürgen Bajorath. Docking and scoring in virtual screening for drug discovery: methods and applications. *Nature reviews Drug discovery*, 3(11):935–949, 2004.

[21] Garrett M Morris, Ruth Huey, William Lindstrom, Michel F Sanner, Richard K Belew, David S Goodsell, and Arthur J Olson. Autodock4 and autodocktools4: Automated docking with selective receptor flexibility. *Journal of computational chemistry*, 30(16):2785–2791, 2009.

[22] Andrew R Leach and Valerie J Gillet. *An introduction to chemoinformatics*. Springer, 2007.

[23] Martin Karplus and J Andrew McCammon. Molecular dynamics simulations of biomolecules. *Nature structural biology*, 9(9):646–652, 2002.

[24] Kota Kasahara, Shun Sakuraba, and Ikuo Fukuda. Enhanced sampling of molecular dynamics simulations of a polyalanine octapeptide: effects of the periodic boundary conditions on peptide conformation. *The Journal of Physical Chemistry B*, 122(9):2495–2503, 2018.

[25] Jian Liu, Dezhang Li, and Xinzijian Liu. A simple and accurate algorithm for path integral molecular dynamics with the langevin thermostat. *The Journal of chemical physics*, 145(2), 2016.

[26] Ulrich Essmann, Lalith Perera, Max L Berkowitz, Tom Darden, Hsing Lee, and Lee G Pedersen. A smooth particle mesh ewald method. *The Journal of chemical physics*, 103(19):8577–8593, 1995.

[27] Md Ataul Islam and Tahir S Pillay. Identification of promising anti-dna gyrase antibacterial compounds using de novo design, molecular docking and molecular dynamics studies. *Journal of Biomolecular Structure and Dynamics*, 38(6):1798–1809, 2020.

[28] Michael K Gilson and Huan-Xiang Zhou. Calculation of protein-ligand binding affinities. *Annu. Rev. Biophys. Biomol. Struct.*, 36:21–42, 2007.

[29] Junmei Wang, Paul Morin, Wei Wang, and Peter A Kollman. Use of mm-pbsa in reproducing the binding free energies to hiv-1 rt of tibo derivatives and predicting the binding mode to hiv-1 rt of efavirenz by docking and mm-pbsa. *Journal of the American Chemical Society*, 123(22):5221–5230, 2001.

[30] Jingxuan Zhu, Congcong Li, Hengzheng Yang, Xiaoqing Guo, Tianci Huang, and Weiwei Han. Computational study on the effect of inactivating/activating mutations on the inhibition of mek1 by trametinib. *International Journal of Molecular Sciences*, 21(6):2167, 2020.

Abbreviations

ANP: Phosphoaminophosphonic acid-Adenylate ester

ERK: Extracellular Signal-Regulated Kinase

GPCR: G protein-coupled receptors

GB: Generalized Born

GTPase: Guanosine triphosphate enzyme

MAPK/MEK: Mitogen-Activated Protein Kinase

MD: Molecular dynamics

MM/PBSA: molecular mechanics/Poisson-Boltzmann surface area

PBC: periodic boundary conditions

PDB: Protein Data Bank

PDBQT: Protein Data Bank with charges and atom types

RCSB: Research Collaboratory for Structural Bioinformatics

RMSD: Root Mean Square Deviation

RMSF: Root Mean Square Fluctuation

RoG: Radius of Gyration

RTK: receptor tyrosine kinases

SASA: Solvent accessible surface area

SMILES: The simplified molecular-input line-entry system

TRA: Trametinib

CV

europass

Lovro Rašan

Nationality: Croatian **Date of birth:** 17/08/1998 **Gender:** Male **Phone number:** (+385) 996970975

Email address: lovrorasan@gmail.com

Home: Jug II/37, 40323 Prelog (Croatia)

ABOUT ME

Education:

1. Department of Biotechnology - University of Rijeka – bacc. Biotech. et pharm. (2020)
2. Prelog High School – General Gymnasium (2017)

Prizes:

1. State competition in biology in research work (2014) - Coverage of macrophytic algae and marine flowering plants in the Adriatic and the island of Gozo in Malta
2. State competition in biology in research work (2016) - Habitats of freshwater jellyfish (*Craspedacusta sowerbyi* Lankaster 1880) in the area of lower Međimurje

Work experience:

1. Elementary school Hodošan - biology teacher (substitute for sick leave)
2. Bioinstitut d.o.o. Čakovec - Professional practice in a chemical laboratory (2020)

Publications:

1. Rašan, D., Marković, S., Dorčić, J., & **Rašan, L.** (2020). Clients' satisfaction with the service provided by pharmacists during the COVID-19 epidemic. Journal of Applied Health Sciences, 6(2), 219–228. doi: 10.24141/1/6/2/4

Participation in scientific meetings:

1. 12th Croatian Biological Congress

Poster-103
M. Rašan, **L. Rašan,** V. Pirc Mezga
Habitats of freshwater jellyfish (Craspedacusta sowerbyi Lankaster 1880) in the area of lower Međimurje

1. 13th Croatian Biological Congress

Poster -119
L. Rašan, L. Hercigonja, M. Rašan
Contribution to the inventory of the flora of Međimurje

Projects:

1. SOS. Blue diving heart
2. Think Green environmental actions

Languages:
Croatian and English

Computer skills:
MS programs, MedCalc, work in Chimera programs, MacMolPlt, gamess

Hobbies:
Mountaineering, skiing and SCUBA diving

Acknowledgements

The author is thankful for good mentor guidance and fast replaying. I would also like to thank my family members (Mišo, Sanja and Dora), best lab partner Leonarda Vučić and roommate Sara Mogorović for mental support during the preparation of the thesis.